The sensitivity of a photoelectric X-ray polarimeter for Astronomy: The impact of gas mixture and pressure

L. Pacciani[*a], E. Costa[a], G. Di Persio[a], M. Feroci[a], P. Soffitta[a], L. Baldini[b], R. Bellazzini[b], A. Brez[b], N. Lumb[b], G. Spandre[b].
[a] Istituto di Astrofisica Spaziale e Fisica Cosmica, CNR,
Via Fosso del Cavaliere 100, I-00133 Roma, Italy
[b] Istituto Nazionale di Fisica Nucleare, sezione di Pisa,
Via Livornese 1291, I-56010, San Piero a Grado (PI), Italy

ABSTRACT

A Micropattern detector in the focus of a grazing incidence telescope is nowadays the most powerful tool to perform a sensitive and reliable measurement of the linear polarization of celestial X-ray sources. The actual implementation of such a completely new device results from a trade-off of various factors and can provide a break-through increase of sensitivity with respect to traditional instrumental approaches. The sensitivity depends on the effective area of the optics and the modulation factor and efficiency of the detector. The latter strongly depends on the filling gas through various factors, including the absorption probability, the length of track versus the pixel size, the blurring introduced by the lateral diffusion during the drift.

We discuss the impact of the choice of the filling gas on the sensitivity and on the operative band of the instrument, while the noble gases drive the efficiency, the organic quenching gases impact both in reducing the scattering and producing most straight tracks and on reducing diffusion. Some design solution are discussed both for a low energy oriented and high energy oriented polarimeters.

Keywords: X-ray astronomy, X-ray polarimetry, gas, mixture, photoelectric, Monte Carlo, simulation.

1. INTRODUCTION

1.1 Photoelectric Polarimetry of X-ray Sources

An extended theoretical literature predicts a high degree of linear polarization in the X-ray emission of celestial sources. This is due either to the emission mechanisms, such as synchrotron, cyclotron, non-thermal bremmstrahlung, or to the scattering of radiation on highly asymmetric systems, such as accretion disks. But the actual implementation of this discipline was relatively deceiving. This is mainly due to the limitation of the conventional techniques based on the Bragg diffraction at 45^{o} or Thomson scattering around 90^{o}. The first polarimeters were flown aboard rockets, and satellites ARIEL-5 and OSO-8. In practices the only positive result, was the detection of polarization by Crab Nebula [1,2] so that no X-ray Polarimeter has been launched since 25 years.

Nevertheless the expectations from such measurement on several astrophysical targets including High and Low Mass X-ray Binaries, isolated neutron stars, Galactic and Extragalactic Black Holes is quite well funded in the frame of current models and a sensitive polarimeter would provide a break-through in the comprehension of the inner regions of compact X-ray sources.

The conventional techniques of Bragg diffraction and Compton scattering are limited, respectively, by the narrow energy band, and the high background. The best implementation of these two techniques is the Stellar X-Ray Polarimeter [3] built for the SPECTRUM-X-Gamma Mission, so far not flown. At higher energy finely subdivision and independent collection of signals provided already an improved design for active Compton polarimeters [4]. At lower

[*] correspondence: E_mail: pacciani@rm.iasf.cnr.it, tel. +39-06-4993-4009

energies, accessible to X-ray optics with medium/large effective area, was recently possible to design and build a finely subdivided, non-dispersive, imaging spectro-polarimeter based on photoelectric effect [5]. This polarimeter provides an enormous jump in sensitivity with respect to different techniques in the same energy bands. The imaging, timing and spectroscopic capability of this polarimeter allows to address most of the expectations of the scientific community. For example it could be possible to disantangle polarization of the jet from the core in AGNs or performing QPO driven polarimetry [6] or spatial-resolved polarimetry of Cluster of Galaxies [7] or in the Galactic center [8] region.

1.2 Statistics

A polarimeter is usually composed of an analyser and a detector. The products of the interaction are distributed in angle around the pointing axis. The counts are modulated in phase with the law :

$$C(\phi) = A + B\cos^2(\phi - \phi_0) \tag{1}$$

where ϕ is the (azimuthal) angle between the projection of the polarization vector on the analyzer and the characteristic axis of the polarimeter and ϕ_0 is the phase angle. The guide-parameter for building a polarimeter is the so called modulation factor μ for a 100% polarized source defined as :

$$\mu = \frac{C_{\max} - C_{\min}}{C_{\max} + C_{\min}} \tag{2}$$

where C_{max} and C_{min} are the counting rate at the fase of the maximum and the minimum, respectively. The relevant statistical parameter is the Minimum Detectable Polarization (MDP) which represents the statistical fluctuation (conventionally fixed at 99 % confidence level) from an unpolarized source:

$$MDP = \frac{4.29}{\mu r}\sqrt{\frac{r+b}{T}} \tag{3}$$

In the present paper we assume that the polarimeter is placed at the focus of an X-ray optics and we specialize the formula of the MDP to such case. Also we are particularly interested in energy resolved polarimeter. T is the integration time, r and b are respectively the source and background counting rate in a selected energy range.

$$r = \int_{E1}^{E2} S(E) * A_{Tel}(E) * \varepsilon(E, P, \mu_{mix}, d, F_{extract}, \mu_{win}, w, F_{cuts}) dE \tag{4}$$

where E is the photon energy in keV, $S(E)$ is the source flux in photons cm^{-2} s^{-1} keV^{-1}, $A_{Tel}(E)$ is the telescope effective area, $\varepsilon(E, P, \mu_{mix}, d, F_{extract}, \mu_{win}, w, F_{cuts})$ is the detector efficiency:

$$\varepsilon = F_{Extract} * F_{cuts} * (1 - e^{-P_{Atm}\mu_{mix}d}) * e^{-\mu_{win}w} \tag{5}$$

which depends on the window absorption μ_{win} and thickness w, on the gas pressure (P), composition (μ_{mix}) and thickness (d), on the typical fraction of the events ($F_{extract}$) included in the extraction radius $R_{extract}$ (e.g. R_{90} is the angular radius which contains 90% of the photons in the Point Spread Function) during the data analysis and finally on the applied cuts, F_{cuts} (if any), and :

$$\mu r = \int_{E1}^{E2} \mu(E) * S(E) * A_{Tel}(E) * \varepsilon(E, P, \mu_{mix}, d, F_{extract}, \mu_{win}, w, F_{cuts}) dE \tag{6}$$

The total background counting rate is the sum of the instrumental residual background, b_{inst} and of the X-ray diffuse background, b_{diff}, integrated in the same extraction area of the focused X-ray celestial source. For a 90 % extraction radius therefore we have (omitting the integral):

$$b = b_{inst} + b_{diff} \tag{7}$$

The contribution of the residual instrumental background to the total background can be evaluated by :

$$b_{\text{int}} = b_{rate} * A_{sens} * (E_2 - E_1) \tag{8}$$

and depends on the gas mixture [9] with a b_{rate} typical value of 10^{-4} counts s^{-1} cm^{-2} keV^{-1} for a Neon based mixture [10]. The sensitive area of the detector depends on the $R_{extract}$ and on the focal length, F_{length}.

$$A_{sens} = \pi(\tan R_{90} * F_{length})^2 \tag{9}$$

$$b_{diff} = \int_{E_1}^{E_2} B_{diff}(E) * \Delta\Omega * A_{Tel}(E) * \varepsilon(E, P, \mu_{mix}, d, F_{extract}, \mu_{win}, w, F_{cuts}))dE \tag{10}$$

$$\Delta\Omega = 2\pi(1 - \cos R_{extract}) \tag{11}$$

For a $R_{extract}$ of 2' (90 % power radius), $\Delta\Omega$ is 10^{-6} steradians and with a 8 m focal length A_{sens} is 0.7 cm^2.

The X-ray diffuse background on one steradian at 1 keV is about at the same level of the Crab. Even for moderate quality optics, a focal plane polarimeter is source dominated down to very small fluxes. In such case, we can define a combination of parameters which maximizes the performances of the polarimeter. We call it the quality factor and use it to compare different configurations :

$$QF = \mu\sqrt{\varepsilon} \tag{12}$$

The QF is energy dependent, therefore we computed its values for various energies for a given design of realistic experiment.

2. BASIC PHYSICAL PROCESSES AND THEIR SIMULATION

2.1 Computational model

A finely subdivided detector, with independent charge-readout, can be used to visualize photoelectron tracks and thence is an excellent polarimeter. The physics behind is well known, and involve photoelectric effect, scattering and slowing of primary electrons in the gas, drift and diffusion, gas multiplication and final collection on a padded readout plane. All these processes are directly or indirectly function of photon energy and of gas parameters such as the composition, the pressure and the gas thickness in a known way. An analytical or semi-empirical approach to determine the quality factor is beyond the scope of this work, and we demanded a characterization of the detector response as polarimeter to a Monte Carlo simulation. Future works on semi-empirical approaches can take advantage of such Monte Carlo results.
Also being the expected polarization of many celestial X-ray sources energy dependent, an accurate determination of the modulation factor as a function of energy is therefore necessary. A calibration facility with known polarized X-ray sources provided with multiple energy lines are, usually, not easily available on a laboratory scale, therefore a Monte Carlo approach, tuned with a sparse-energy calibration points, is indeed desirable.

In the Monte Carlo we describe the processes in a Micro Pattern polarimeter [11]. A photoelectron is absorbed in a gas and the electrons are transferred by a parallel, constant field to a detecting plane subdivided into hexagonal pads.

2.2 Photoelectric interaction with the target gas

The basic radiation-matter interaction exploited for measuring the X-ray polarization is the photoelectric effect.We distributed the absorptions along the active region of the detector according to :

$$a = e^{-\mu_{mix} d} \tag{13}$$

The angular distribution of a s-photoelectron is modulated by the polarization of the incoming photon. According to the non relativistic approach [12], the angular distribution is given by :

$$\frac{\partial\sigma}{\partial\Omega} = r_0^{\,2}\,\frac{Z^5}{137^4}\left(\frac{mc^2}{h\nu}\right)^{7/2}\frac{4\sqrt{2}\sin^2(\theta)\cos^2(\varphi)}{(1-\beta\cos(\theta))^4} \tag{14}$$

where r_o is the classical electron radius, Z is the atomic number of the target material and β is the electron velocity in fraction of the speed of light c. The figure 1 (left) shows the meaning of the emission angle θ and azimuth angle φ, while figure 1 (right) shows the differential cross section $d\sigma/d\theta$ showing how the photoelectrons are mostly ejected in a

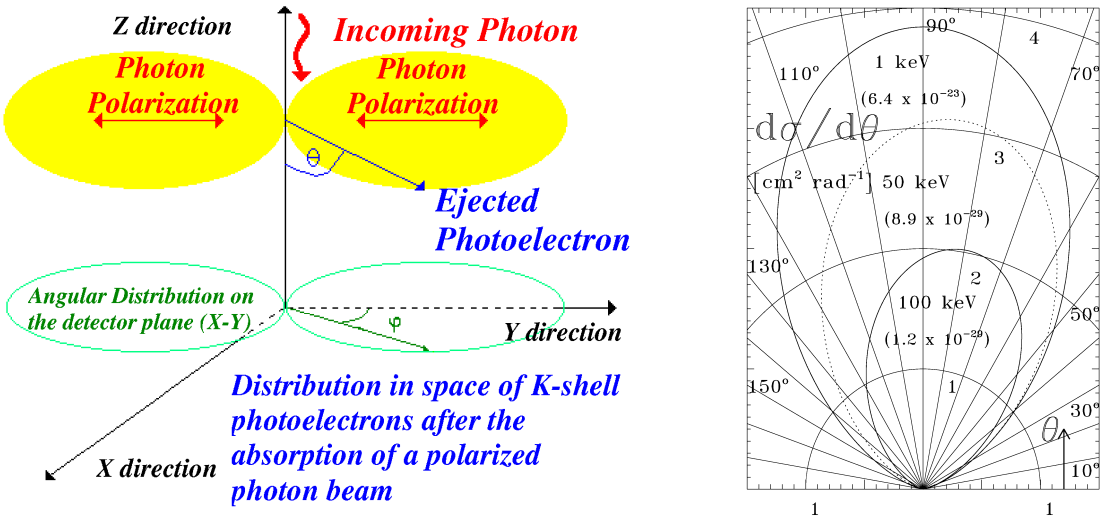

Fig.1 (Left) Artistic view of the photoelectric effect . (Right) Differential cross-section with respect to the emission angle for a Neon atom. In brackets are shown the factor for which each energy involved in the calculation must multiply the iso-curve (with value 1,2,3 and 4). About 50% of photoelectrons are, at low energies, ejected between 60° and 120° . The forward

plane perpendicular to the direction of the incoming photons. Being the cross-section a rapidly decreasing function of the photon energy and a rapidly increasing function of the atomic number, for each energy band, typically not larger than a decade, there is suitable gas mixture to be used. The choice of the gas mixture is also driven by the following considerations:

(i) The p-photelectron and the d-photoelectron are less modulated with respect to s-photolectrons [13]. The highest modulation factor, for the same energy difference with the corresponding shell (K or L) is therefore obtained by operating above the K-shell. A low Z gas mixture is therefore preferable.

(ii) The Auger electrons angular distribution are, in general, not modulated by the polarization of the X-rays, therefore the operative energy range is at least twice the K absorption edge. Being the Auger electron energy larger for a larger Z atom, a low Z gas mixture is preferable.

We simulated both the photoelectron angular distribution following the K-shell absorption and the angular distribution following the L shell (L_{III}) absorption, deriving the relative probability from the jump in the cross section at the K-edge.

We assign to the Auger electrons the energy of the corresponding shell and an isotropic distribution. The fluorescence is assumed to escape the region of interest. We used the fluorescence yields showed in Bambynek et al.[14] and cross section in Veigele [15] for energy below 1 keV and by using XCOM [16] for energy over 1 keV. Some of the assumption we made are crude, however we are confident we provided a realistic simulation of the interaction. In the energy range accessible to 'classical' X-ray optics, suitable gas foresee the use of neon-based mixture or hydrocarbon gas like propane or iso-C_4H_{10}. In hard X-ray applications, instead, a larger Z gas mixture, for example Argon-based or Xenon-based mixture can be devised. The choice of the gas mixture is a trade off to provide the best quality factor in the given energy range.

2.3 Photoelectron and Auger electron propagation in the gas mixtures

The core of the Monte Carlo code for the transport of the photoelectron and of the Auger electron was developed by D. Joy [17]. Physical processes taken into account for the electrons propagation were single elastic scattering of the electron with the electric field of the nuclei and the energy loss due to the ionization/excitation of the medium. For the elastic scattering, Joy used the Browning parametrization of the total elastic Mott cross section:

$$\sigma_M(cm^2) = 4.7\times10^{-18}\frac{\left(Z^{1.33}+0.032Z^2\right)}{\left(E+0.0155Z^{1.33}E^{0.5}\right)}\frac{1}{\left(1-0.02Z^{0.5}e^{-u^2}\right)} \tag{15}$$

Where E is the electron energy in keV, and $u = \log_{10}(8.EZ^{-1.33})$.

The scattering angle ϕ is generated with the following algorithm:

$$\cos(\phi) = 1 - \frac{2\alpha RND^Z}{(1+\alpha-RND)} \tag{16}$$

where α is the screening factor.

The original Monte Carlo was developed to transport electrons in a monoatomic medium, we generalized the original code to treat the propagation in gas mixtures. The mean free path between two elastic scattering in the mixture is calculated as

$$\frac{1}{\lambda} = \sum_i \frac{1}{\lambda_i} \tag{17}$$

Where the sum is extended to every element of the gas mixture.

The transport algorithm performs the following steps:

1. extracts the distance travelled by the electron from the current position to the next elastic scattering,
2. extracts the atom responsible for the scattering (the probability of the atom *i* is λ/λ_i),
3. extracts the new direction of the electron according to the Mott cross section for the chosen atom,
4. decreases the electron energy of the amount lost with the ionisation/excitation of the medium travelled between two elastic scattering, using a modified Bethe function for low-energy application in a gas mixture.

5. stops the tracking if the electron energy is below 50 eV (else goes to the step 1).

The simulated track of a photolectron and of a Auger-electron, generated by an X-ray with an energy of 8 keV, is shown as solid track in figure 2 (left).

2.4 Transport of ionization secondary charges and the detector response

After we computed the local energy loss, we convert it into secondary electrons (taking into account the average energy required to produce elecron-ion pair). Every secondary electron is drifted to the detecting plane. During the drift it is diffused in the transverse direction assuming a gaussian distribution with

$$\sigma_{diffusion} = \sigma_{1cm}\sqrt{d(cm)} \qquad (18)$$

where *d* is the distance travelled by the secondary electron along the electric field from the production point to the detection plane, and σ_{1cm} is the R.M.S. transverse diffusion after 1 cm of drift. The effects of the Gas Electron Multiplier is neglected since it does not change the shape. In the following calculation we used the indicated σ_{1cm} :

Gas Mixture	σ_{1cm} at 1 atm (μm)
iso $-C_4H_{10}$	100
Ne 80% + DME 20%	80
Ne 20% + DME 80%	60
Ar 80% + CH_4 20%	220
Ar 80% + C_3H_8 20%	120

Table 1., compilation of the r.m.s. transverse diffusion used in our Monte Carlo simulation.

The values in the table are taken from Peisert and Sauli [18], while values for mixtures and pressures not provided were interpolated or extrapolated from known values.

The signal of a pad is simply defined as the number of diffused electrons impinging on it in a single photoelectric interaction, therefore the multiplication of the GEM and the electronic noise were not taken in account. The eventual result of the Monte Carlo is a set of pads each with the assigned charge. The simulated track as detected by the Micro Pattern is showed as squares in figure 2 (left).

2.5 Reconstruction of the photoelectron initial direction

The algorithm of reconstruction of photoelectron is based on the procedure described in the paper by Bellazzini et al.[19]:

1. calculation of the charge-barycentre of the cluster,
2. determination of the major and minor axis of the cluster,
3. identification of the region containing the initial part of the track (the minor axis divide the cluster in two regions of different energy density, the *minor density region* is selected),
4. selection of the *most distant pad* from the barycentre,
5. selection of the pad, the *point zero pad,* containing the maximum energy deposit (corresponding with the region of emission of Auger electron. The *point zero pad* is chosen in a circle around the *most distant pad*),
6. estimation of the *impact point* as the energy barycentre calculated in another circle around the *point zero pad,*
7. recalculation of a new major axis (of the *minor density region)* from the *impact point.* This axis is considered the photoelectron *initial direction.*

We stress that this procedure is well suited for the Ne + DME mixture, where the Auger electron has a very low energy, compared with the energy of the photoelectron, and it can fail for higher-Z mixture or in proximity of the K-edge. In spite of this, the same algorithm is used for all the mixtures analysed in this paper.

The modulation curve is the histogram of the distribution of the estimated *initial direction* and it is shown in figure

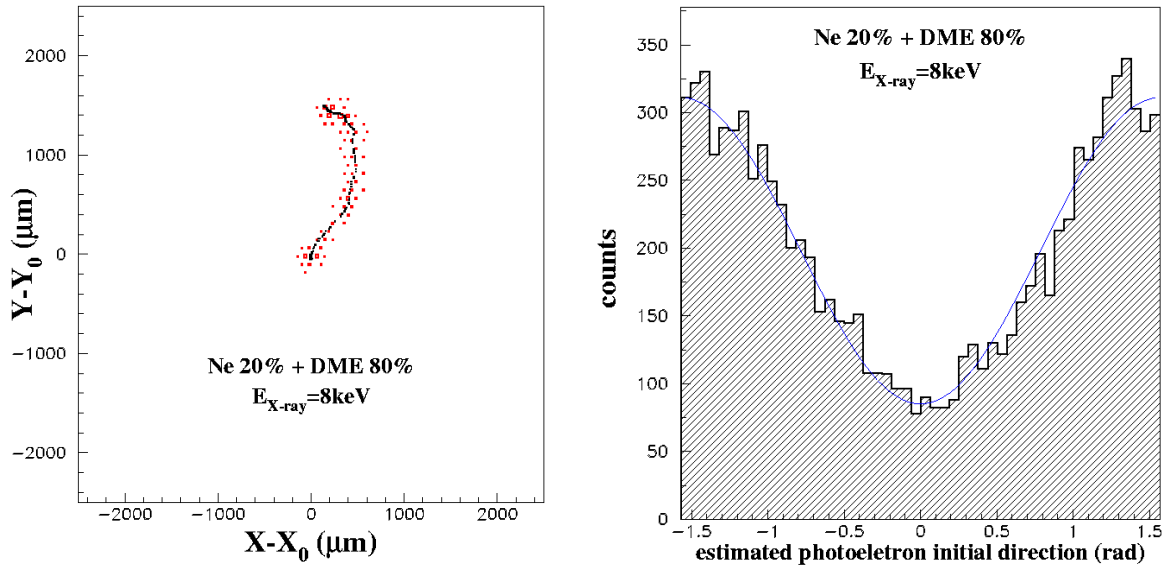

Figure 2. (Left) Simulated photo-electron and Auger electron track (solid) blurred by the diffusion in the drift towards the detector plane (squares). (Right) Modulation curve obtained by estimating the initial direction of the photoelectron track.

2 (right) for an X-ray of 8 keV absorbed in a Ne+DME mixture.

3. SENSITIVITY CALCULATION FOR A SET OF SUITABLE GAS MIXTURE

All the described machinery were used to estimate the modulation factor for various gas mixtures. We simulated the interaction of the primary X-ray with the target gas mixture with the relative cross section for each component of the gas mixture at the given energy. Then we simulated the angular distribution and the propagation in the gas of the photoelectron and of the Auger electron, and finally the collection on the hexagonal pads of the readout plane, which is our detector response. The modulation curve obtained as histogram of the estimated initial direction of the photoelectron track was fitted with the formula (1) in order to calculate the modulation factor as in formula (2). As a comparative work we choose gas mixtures with increased average atomic number in order to evaluate the sensitivity of the polarimeter in a large energy band. We also explored the effect of different gas thickness and pressure in order to estimate good configurations for a focal plane experiment. In table 2 we show the mixtures and the configurations used. They span from a relatively low-Z, low-pressure gas for low energy applications, with small diffusion coefficient (iso-C_4H_{10}) to Ne-DME in two different relative percentage. Finally, for high energy applications, Ar-C_3H_8 is compared with Ar-CH_4. We modeled the readout plane with hexagonal pads having 100 μm pitch. We first evaluated the modulation factor (fig. 3-7, left panels) then we calculated the quality factor *QF* (fig. 3-7, right panels). In figure 8 we compared the QF for our set of mixtures with representative parameters.

Gas	Pressure (atm)	Gas thickness (cm)	Energy (keV)
iso-C_4H_{10}	1/16 , 1/8	0.5 , 1 , 2	0.3 , 0.5 , 0.7 , 1 , 1.5 , 2 , 4 , 6
Ne 20% + DME 80%	0.5 , 1	0.5 , 1 , 2	1 , 2 , 4 , 6 , 8 , 10 , 12
Ne 80% + DME 20%	0.5 , 1	0.5 , 1 , 2	1 , 2 , 4 , 6 , 8 , 10 , 12
Ar 80% + CH_4 20%	2	2	4 , 8 , 12 , 16 , 20 , 24 , 30
Ar 80% + C_3H_8 20%	1 , 2 , 4	1.5 , 2 , 3	4 , 8 , 12 , 16 , 20 , 24 , 30

Table 2 Set of gas mixtures, gas thickness and energies used in our simulation.

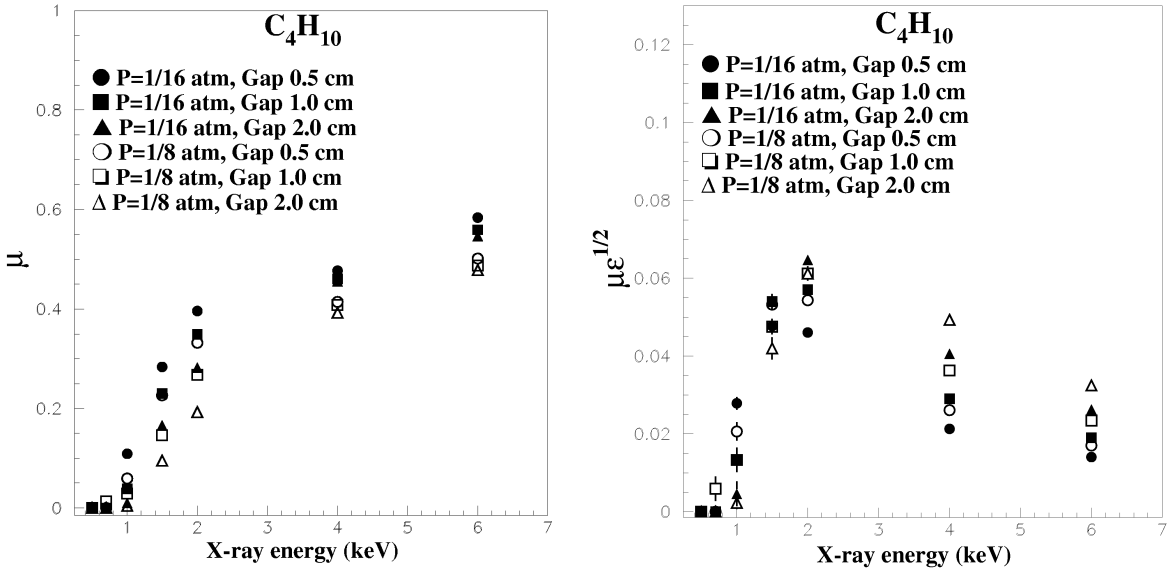

Figure 3. (Left) Modulation factor, μ, and (right) quality factor, *QF*, for iso-C_4H_{10}, mixtures. A multilayer polyimide window, 900 nm thick, with W strongback is considered in the evaluation of the efficiency.

We made some assumption on the entrance windows:

- for isobutane we considered a multilayer window (PG-W) of 900 nm thickness with transmissions provided by the producer (Metorex OY), included a 0.95 transmission polyimide grid and a 0.88 transmission W grid.
- for Ne + DME mixtures we adopted a Be window of 50 μm,
- for Ar + CH_4 and Ar + C_3H_8 we considered a Be window. The chosen thickness was 50, 100, 200 μm for use with gas at 1, 2, 4 atm respectively.

We want to stress here that all the set of data are processed in the computations, and for our comparative work no cuts were applied to the simulated data. However we already know that cuts, for example, in the shapes of the tracks, provide a higher μ.

For all the mixtures we investigated, the modulation factor is higher at higher energies, for thinner gas gap and for smaller pressures. As expected a larger mean atomic number provides a higher low-energy threshold for polarimetry sensitivity. Iso-C_4H_{10} provides the better modulation factors at low energy, Neon-based mixtures, in the intermediate energy region, with larger DME content, provides larger modulation factors because of the larger braking/scattering ratio and for the smaller diffusion coefficient.
The modulation factors obtained for Ar+C_3H_8 are better than those obtained for Ar+CH_4 due to the larger diffusion coefficient for the latter.

The quality factor *QF* is instead a function with a maximum in the energy range explored by our simulations for all the mixtures we investigated. Infact the sensitivity rises sharply to a maximum obtained at 2 keV for iso-C_4H_{10}, 4 keV for Ne-based mixtures, while for Ar-based mixtures rises more smoothly to the maximum obtained at 8-10 keV.
At lower energies, where the gas efficiency is larger, a better sensitivity is obtained by smaller gaps and pressure because of the larger modulation factor, at higher energies a better sensitivity is obtained by larger gaps and larger pressures because of the better efficiency compared to the increased modulation factor.

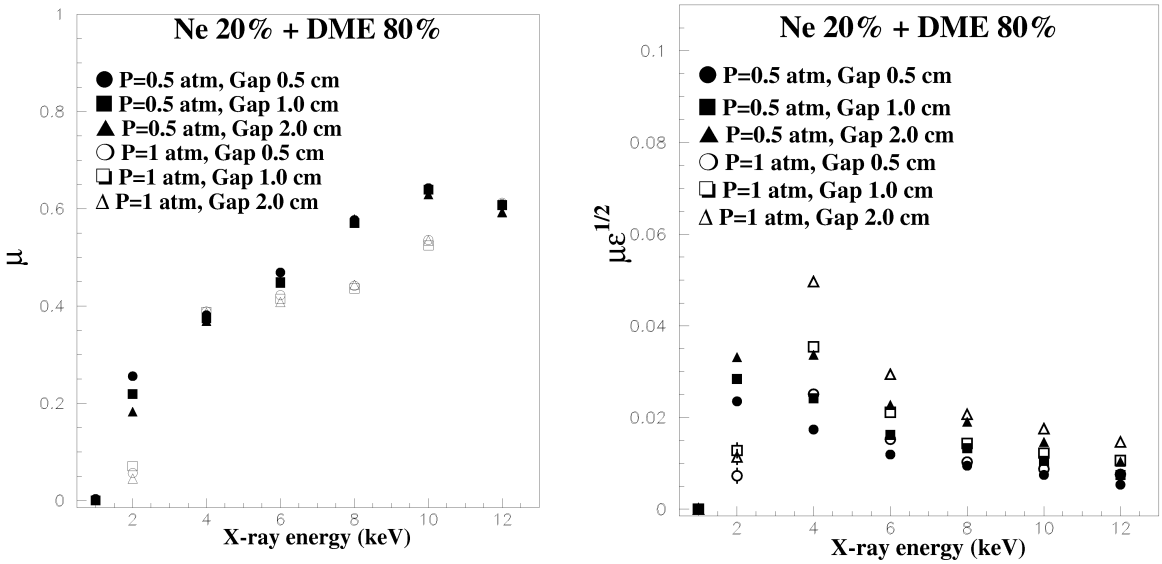

Figure 4. (Left) Modulation factor, μ, and (right) quality factor, *QF*, for a Ne-based mixture. A beryllium window 50 μm thick is considered in the evaluation of the efficiency.

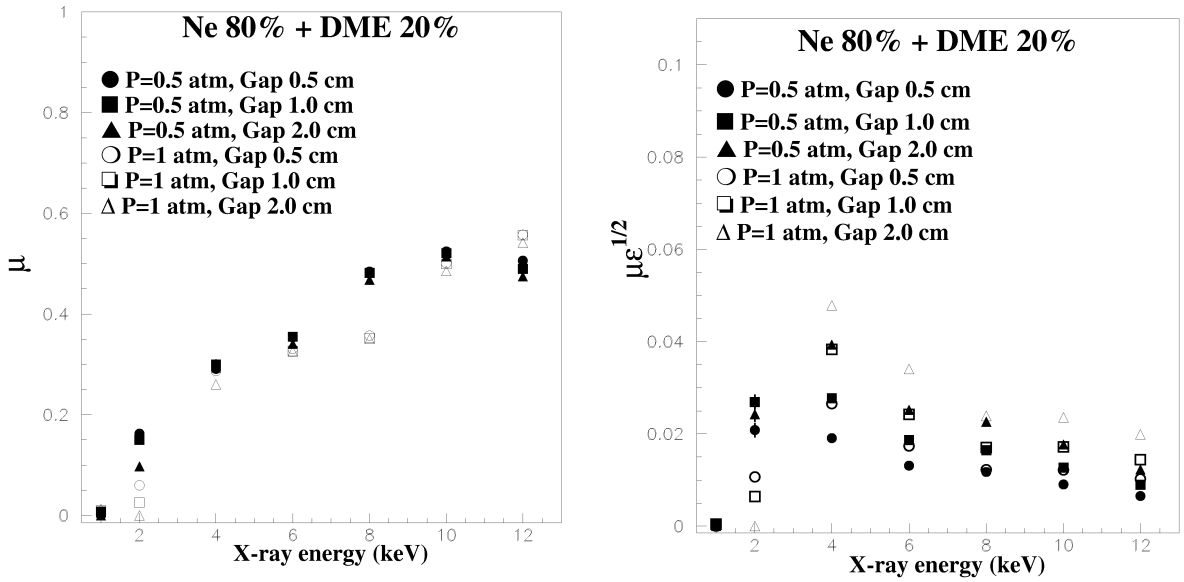

Figure 5. (Left) Modulation factor, μ, and (right) quality factor, *QF*, for a Ne-based mixture. A beryllium window 50 μm thick is considered in the evaluation of the efficiency.

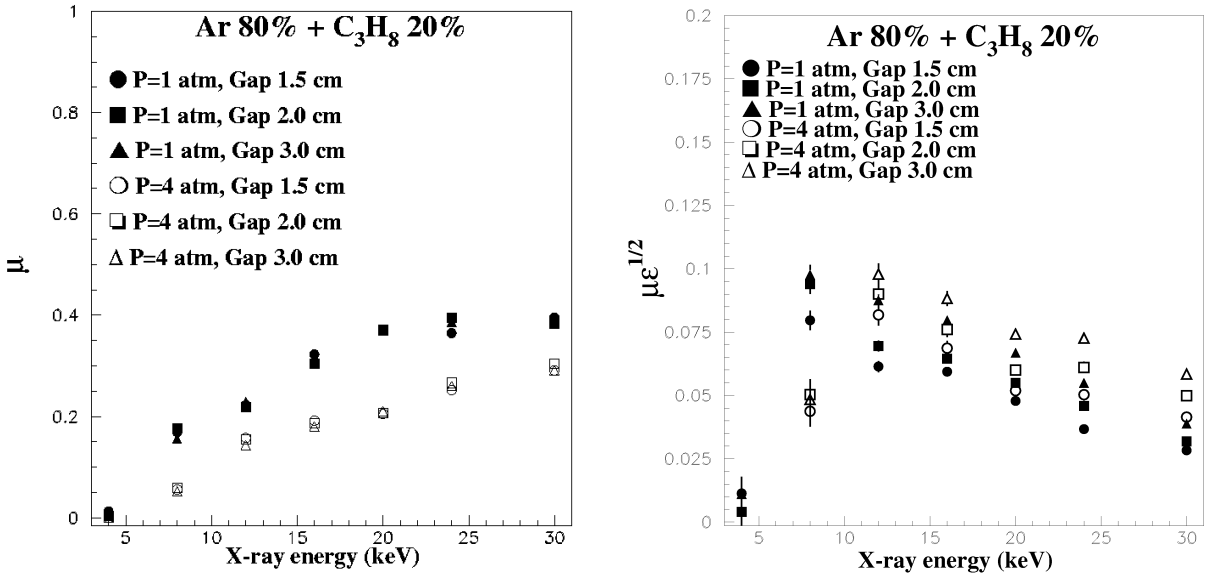

Figure 6. (Left) Modulation factor, μ, and (right) quality factor, *QF*, for a Ar-based mixture. A beryllium window 50 μm (1-atm) thick and 200 μm (4-atm) are considered in the evaluation of the efficiency.

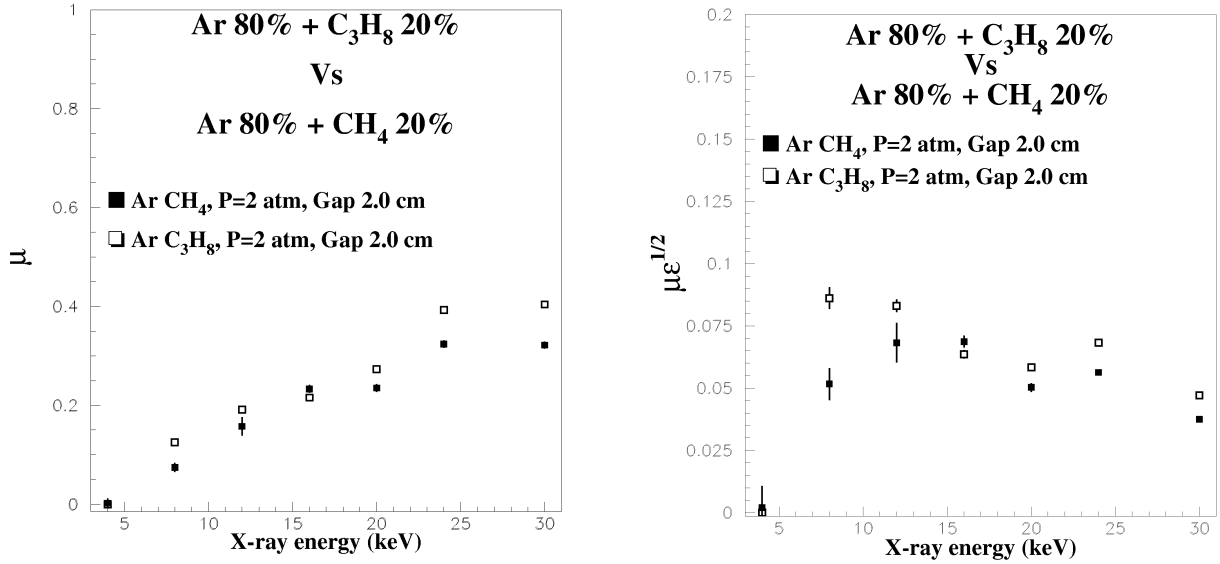

Figure 7. (Left) Modulation factor, μ, and (right) quality factor, *QF*, for two Ar-based mixtures. A beryllium window 100 μm (2-atm) thick are considered in the evaluation of the efficiency.

We finally present a comparative plot of the quality factor, QF, for three representative gas mixtures. The increasing low-energy threshold with the atomic number is clearly visible, suggesting that better performances in a wide energy band can be obtained by means of a composite polarimeter. The argon based mixtures obtained the highest quality factors.

In our comparative work we did not attempted to provide better algorithms, tuned with the gas mixture under study and with the energy region explored. This is a topic of another paper [19] . We also gave-up any tentative of pattern recognition and we remand the reader to future works on this subject.

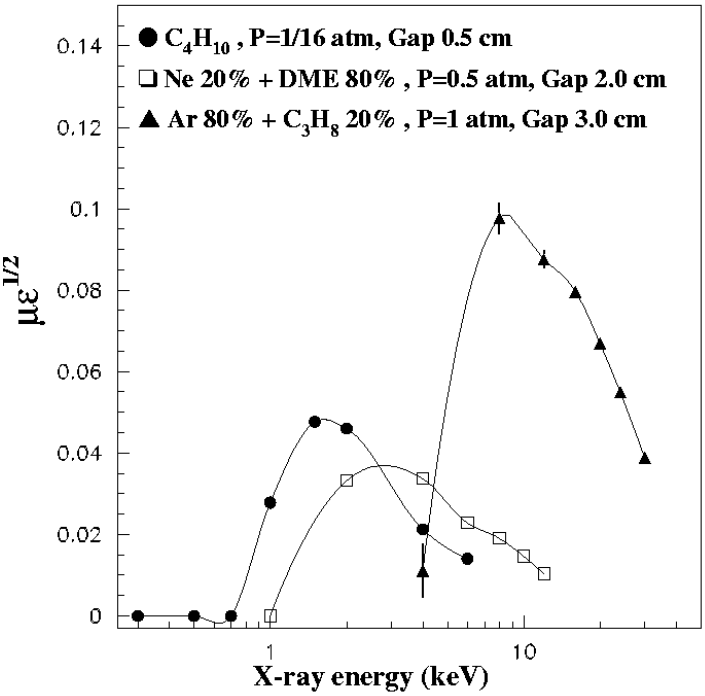

Figure 8. Quality factor for three representative mixtures.

4. CONCLUSIONS

From this preliminary analysis we can sketch some partial conclusions. The first, qualitatively trivial but quantitatively proofed, is that similar mixtures can result in significantly different performances. It is the case of Argon-Methane versus Argon-Propane, very similar for the detecting properties. The latter is significantly better, because the quencher makes the tracks straighter and reduces the transverse diffusion: the optimisation can be a matter of details.

The photoelectric polarimeter is a wide band instrument if compared with the Bragg polarimeter but, for sure, a filling mixture optimal on a broad band does not exist. Photoelectric cross section decreases with the third power of the photon energy. This means that if we want a reasonable efficiency at higher energies only a thin layer, opposite to the collecting plane, is involved in the detection of low-energy photons: if we increase the sensitivity at higher energies we decrease the sensitivity at low energies because the diffusion smears the modulation. From figure 8 we would say that an organic mixture is better for low energies (<1 keV to 2 keV) and the optimal gas should be selected on the basis of diffusion. At higher energies (> 6 keV) the Ar seems a good basic ingredient for filling mixtures up to high energies (20-25 keV) and thence seems a good filler for an experiment based on multi-layer optics. A Ne-DME mixture (with some preference for a larger content of the quencher) seems good as intermediate device, still effective at 8 keV but with some sensitivity at low energies (2 keV or even less). Data suggest that even an absorption gap thicker than 20 mm could be acceptable, even though not included in simulations. As a very preliminary result, we would say that if a single detector is to be positioned in the focus of an optics, a Ne based mixture is the best choice. If one can afford two

polarimeters, sharing the observing time, a combination of a Argon based detector and an all-organic detector is the configuration that provides the best wide band performance.

Our simulations fix the pixel size of 100 μm. In an actual optimisation this can vary from 50 to 200 μm impacting on the low energy performance (but also on the constraints to the experiment). Another point is that our data are affected by the window selected. In a real case the window design should be part of the experimental trade-off. Another topics deserving future work is the pattern recognition. It can be extremely important for energies close to the K-edge where the Auger electron and the photoelectron are comparable.

We conclude that much work is still to be done to arrive to a photoelectric polarimeter optimised for a certain optics and for a certain class of astrophysical targets.

AKNOWLEDGEMENT

This work is partially funded by the Italian Space Agency (ASI).

REFERENCES

1. R. Novick, M.C. Weisskopf, R. Berthelsdorf, R. Linke and R.~S. Wolff, Astrophys. J. **74** (1972) L1.
2. M.C. Weisskopf, E. Silver , H.L. Kestenbaum, K.S. Long, R. Novick , Astrophys. J. **220** (1978) L117.
3. P. Kaaret, J. Schwartz, P. Soffitta, J. Dwyer, P. Shaw, S. Hanany, R. Novick, R. Sunyaev., I. Lapshov, E. Silver, K. Ziock, M.C. Weisskopf, R.F. Elsner, B. Ramsey,, E. Costa, A. Rubini, M. Feroci, L. Piro, G. Manzo, S. Giarrusso, A. Santangelo, L. Scarsi, G.C. Perola, E. Massaro, G. Matt, SPIE, **2010** (1993) 22.
4. E. Costa, M.N. Cinti, M. Feroci, O. Matt, M. Rapisarda, Nucl. Inst. Meth. A **366**, 1995, 161.
5. E. Costa, P. Soffitta, R. Bellazzini, A. Brez, N., Lumb and G. Spandre, Nature, **411**, 2001, 662.
6. S.Y. Sazonov,A. Churazov R.A. Sunyaev Mon. Not. R. Astron. Soc., **333**, 2002, 191.
7. S.Y. Sazonov, R.A. Sunyaev, Astron. Astrophys, **373**, 2001, 372.
8. E. Churazov, R. Sunyaev, S. Sazonov, Mon. Not. R. Astron. Soc., **330**, 2002, 817.
9. M. Feroci, E. Costa, J. Dwyer, E. Ford., P. Kaaret, M. Rapisarda, P. Soffitta, NIM A **371,** 1996, 538.
10. A. N. Bunner, Astrophys. J., **220**, 1978, 261.
11. R. Bellazzini, F. Angelini, L. Baldini, A. Brez, E. Costa, G. Di Persio, L. Latronico, M.M. Massai, N. Omodei, L. Pacciani, G. Spandre, 'A Micro Pattern Gas Detector for X-ray polarimetry', proceedings of SPIE conference, **4843**, Waikoloa, 2002.
12. W. Heitler, ' The quantum Theory of Radiation', Dover Publications, 1954, New York.
13. A.M. Afanas'ev, R.M. Imanov, É. M. Pashaev, V.N. Peregudov and M.I. Abdullaev, Sov. Phys. Solid State **30**(6), 1988, 1004.
14. W. Bambynek, B. Crasemann, R.W. Funk, H-U. Freund, H. Mark, C.D. Swift, R.E. Price, P. Venugopala Rao, Rev. of Mod. Phys., **14,** 1972, 716.
15. WM. J. Veigele, Atomic Data Tables, **5**, 1973, 51
16. XCOM: NIST Standard Reference Database 8 (XGAM) http://physics.nist.gov/PhysRefData/Xcom/Text/XCOM.html
17. D. C. Joy,' Monte Carlo Modeling for Electron Microscopy and Microanalysis', Oxford University Press, 1995, New York.
18. A. Peisert and F. Sauli,'Drift and Diffusion of electrons in gases: a compilation', CERN report 84-08, 1984
19. R. Bellazzini , F. Angelini, L. Baldini, A. Brez, E. Costa, G. Di Persio, L. Latronico, M.M. Massai,N. Omodei, L. Pacciani, G. Spandre, 'A novel gaseus X-ray polarimeter: data analysis and simulation', proceedings of SPIE conference, **4843**, Waikoloa, 2002.